Journal of
Marine Science and Engineering

MDPI

Article

Deciphering Paleoceanographic Shifts Inferred from the Foraminiferal Record of the Western Svalbard Slope (Bellsund Drift) over the Past Century

Viviana M. Gamboa Sojo [1,*], Caterina Morigi [2,*], Leonardo Langone [3] and Renata G. Lucchi [4]

[1] Escuela Centroamericana de Geología, University of Costa Rica, San José 11501-2060, Costa Rica
[2] Department of Earth Sciences, University of Pisa, 56126 Pisa, Italy
[3] Institute of Polar Sciences, Italian National Research Council (CNR-ISP), 40129 Bologna, Italy; leonardo.langone@cnr.it
[4] National Institute of Oceanography and Applied Geophysics (OGS), 34010 Sgonico, Italy; rglucchi@ogs.it
* Correspondence: viviana.gamboasojo@ucr.ac.cr (V.M.G.S.); caterina.morigi@unipi.it (C.M.)

Abstract: The objective of this study was to reconstruct the last century's climatic oscillations in the Arctic region around the Fram Strait using high-resolution analysis of foraminiferal assemblages as proxies for surface and deep-water mass properties. In this area, warm Atlantic water masses are advected to the Arctic Ocean through the West Spitsbergen Current, representing the northernmost tip of the Global Thermohaline Circulation. The interaction between the cold Arctic and the warm Atlantic water masses significantly influences the entire foraminiferal community. Planktic species such as *Neogloboquadrina pachyderma* and *Turborotalita quinqueloba* are respectively used as indicators of cold Arctic water and warm Atlantic water masses. Among the main benthic species, *Cibicidoides wuellerstorfi*, *Epistominella exigua*, and *Oridorsalis tener* stand out, serving as proxies for the bottom water mass current velocity and paleoproductivity. The paleoenvironmental reconstruction obtained with the foraminiferal assemblages, together with data from satellite monitoring of the sea ice extent and the long-term record of the annual temperature of the West Spitsbergen Current measured over the last 50 years, support the evidence of a progressively rising heat influx into the Arctic Ocean due to an increasing Atlantic water inflow, forcing the consequent decay of the sea ice extent.

Keywords: planktic and benthic foraminifera; sea ice; Svalbard; last century

Citation: Gamboa Sojo, V.M.; Morigi, C.; Langone, L.; Lucchi, R.G. Deciphering Paleoceanographic Shifts Inferred from the Foraminiferal Record of the Western Svalbard Slope (Bellsund Drift) over the Past Century. *J. Mar. Sci. Eng.* **2024**, *12*, 559. https://doi.org/10.3390/jmse12040559

Academic Editor: Petra Heinz

Received: 27 February 2024
Revised: 20 March 2024
Accepted: 21 March 2024
Published: 27 March 2024

1. Introduction

The Bellsund contouritic drift, located on the western margin of Svalbard, was shaped through time by the northward-flowing West Spitsbergen Current (WSC), representing the northernmost tip of the Global Thermohaline Circulation transporting warm North Atlantic water to the Arctic region. The Bellsund Drift experiences cyclic sediment replenishment by the WSC, generating a continuous, high-resolution sedimentary sequence containing details of the depositional history [1] and information on past climatic fluctuations spanning multiple decades throughout recent centuries. The historical records of glaciers in this area document the large growth of sea ice observed during the Little Ice Age (1500 to 1890 AD) [2,3]. A previous study emphasised the strong need for high-resolution studies specifically targeting decadal climate shifts in the Late Holocene, aiming for a better understanding of the climate variability within the Svalbard region [4].

1.1. Oceanographic Settings

The Fram Strait, located between Greenland and Svalbard, represents the only deep gateway connection between the Arctic and North Atlantic Oceans. Here, the surface and warm Atlantic water (AW) is transported northwards by means of the WSC flowing along the eastern side of the Fram Strait. In the deeper part of the water column, the Norwegian

Sea Deep Water (NSDW), located between 1000 and 1800 m water depths, constitutes the colder and slower, deeper core of the WSC that allows the deposition of the sediment drifts. On the western margin of the Fram Strait, the cold and fresher Arctic water flows southwards along the eastern margin of Greenland, taking the name of the East Greenland Current (EGC) [5–7] (Figure 1). The interaction between the surface WSC and the EGC water masses creates the Polar Front, which determines a strong salinity and temperature gradient between the two oceans, influencing the climate of the entire Arctic region [8]. The inflow of warm Atlantic water into the Arctic Ocean throughout the Fram Strait and the Barents Sea is about 5–10 times larger than the inflow of the shallow Pacific water through the Bering Strait [8–10]. The WSC entering the Arctic Ocean loses heat and salt, splitting into several minor branches, one of which turns back along the eastern margin of Svalbard, transporting a modified colder and fresher Arctic water (ArW) through the East Spitsbergen Current (ESC) (Figure 1). Recent studies indicated that the intensified heat flux to the Arctic is directly linked to the reduction in ice cover observed in recent years [11–13], and the progressive heating produces an alteration in the nutrient dynamics and primary production, along with instability in the seasonal cycle of the region [14–16]. This hydrographic configuration controls the presence and extension of the seasonal sea ice on the western margin of Svalbard [4]. Studies performed in this area report a highly variable location of the sea ice margin in the winter during the last ca. 150 years, with persistent evidence of ice retreat [17] or a lack of sea ice in the western Svalbard area during the last 200 years [18]. Spielhagen et al. [19] indicated an increasing trend for the ocean temperatures, showing that an unprecedented warming of the AW occurred during the past 200 years. Tesi et al. [20] dated the onset of the Atlantification to the early 20th century, with a consistent amplification during the most recent period.

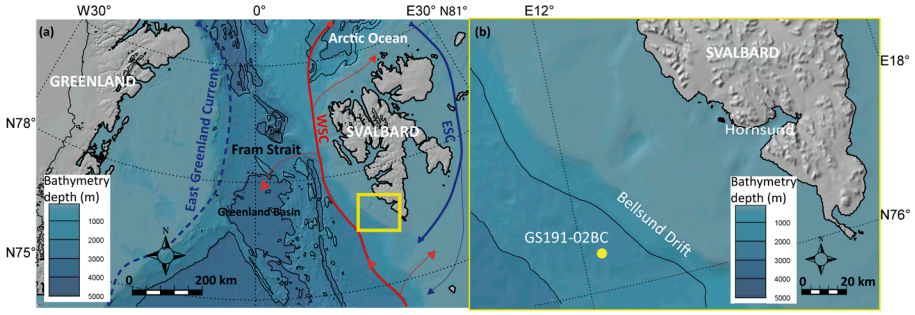

Figure 1. Study area showing the location of the box-core GS191-02BC. (**a**) Location map showing the Svalbard archipelago and the study area (yellow square), with the main currents: WSC (West Spitsbergen Current, red arrow), ESC (East Spitsbergen Current, blue arrow), EGC (East Greenland Current, blue dashed line). (**b**) Bathymetrical map of Bellsund Drift showing the box-core site (yellow dot).

1.2. Temperature and Sea Ice Record in the Fram Strait from Satellite Monitoring

The ocean temperature, the sea ice extent, and the sea ice thickness represent important climate indicators linked to dynamic and thermodynamic processes. The extent of the sea ice in the area appears to have been strongly impacted by the thermal effect of the currents since 1860 [17]. Among the main factors that affect the sea ice extent are the sea and air temperatures. Their inter-annual changes can affect the growth and the persistence of the sea ice. Warmer temperatures during the winter season can inhibit the sea ice extent, whereas high temperatures during the summer can accelerate the melt and demise of the ice cover on land [21]. Spielhagen et al. [19] indicated that the mean temperature values for the Modern Period (since 1890) exceed the temperatures of the last 2000 years, and the superficial water has become warmer, which is in accordance with the consistent retreat of the sea ice in the studied area [18].

Hydrographic surveys in the Fram Strait started in 1910 with the primary objective of documenting the WSC temperature. However, it is important to note that there are gaps in

the recorded data from 1926 to 1962 and from 1964 to 1973 (https://mosj.no/en/, accessed on 18 March 2024). Since 1979, monitoring of the sea ice extent around Svalbard has been carried out using satellites. The whole monitoring record clearly indicates a consistent diminishing trend in the sea ice extent, resulting in the southern area having sea-ice-free conditions, also affecting the region of the Bellsund Drift (https://mosj.no/en/) (Figure 2), with a sea ice loss rate of approximately 13% per decade since the beginning of satellite monitoring. This general reduction in the sea ice extent has also led to the shrinking and thinning of ice floes, consequently allowing more sunlight to penetrate deeper into the ocean. The continuous dataset from 1963 reveals a notable increase in the WSC temperature, rising from 4.4 °C in 1963 to 5.8 °C in 2016 (Figure 2).

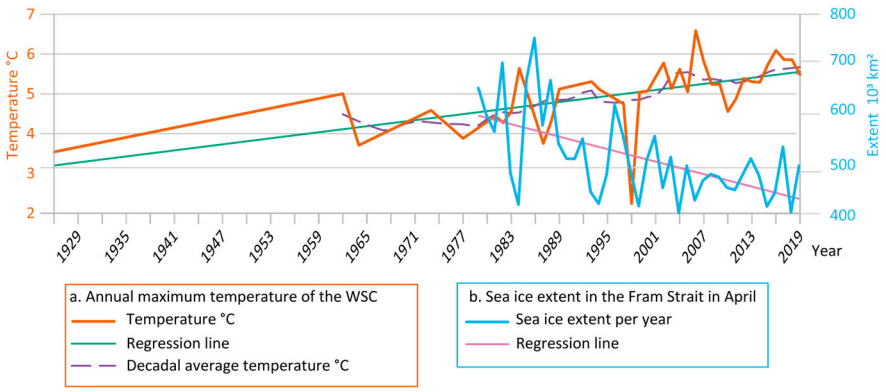

Figure 2. On the left axis is the annual maximum temperature (orange line) of the West Spitsbergen Current (WSC). The decadal average temperature of the WSC from 1962 is indicated by the dashed purple line, (temperature in °C); the linear regression of the WSC temperature (green line) is also indicated. On the right axis, the sea ice extent is represented in units of 10^3 km^2 for the Fram Strait during the last 50 years in April, the month associated with the maximum extent (pink line); the linear regression of the sea ice extent is indicated by the yellow line. Database: Norwegian Polar Institute (2020).

2. Materials and Methods

The box-core GS191-02BC was collected on the crest of the Bellsund Drift during the EUROFLEETS-2 Cruise PREPARED on board of the R/V G.O. Sars during June 2014 (Table 1). The recovery of the sediment was carried out using a box-corer with a 30 × 30 × 50 cm steel box to ensure the recovery of the uppermost part of the sedimentary record [22]. The lithological description was carried out on board during the oceanographic campaign. The sediment recovered in the box-core was formed at the base by slightly bioturbated silty clay (25–5 cm below sea floor (bsf)) topped by soft, brown silt and silty clay, containing abundant bioclasts and sparse ice-rafted debris (IRD) (5–0 cm bsf) [22] (Figure 3). Six subsamples were collected from the box-corer using plastic liners. For this study, one core (sediment recovery 19 cm) was selected for micropaleontological, grain size, and ^{210}Pb analysis, and one core (sediment recovery 22 cm) was used for XRF core scan analyses, core photographs, and X-radiography.

Table 1. General information on the box-core used for this study (see Lucchi et al. [22] for further details).

Core Code	Type of Sampler	Coordinates	Water Depth (m)	Maximum Sediment Recovered (cm)
GS191-02BC	Box-corer	76° 31.30′ N 12° 44.29′ E	1647	25

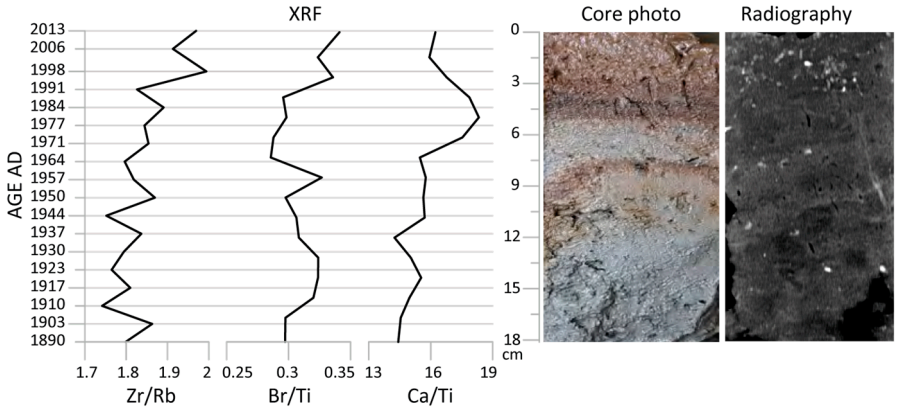

Figure 3. Downcore distribution of the XRF element ratios, compared with the core BC-02 photograph and radiography. In the radiography, a lighter colour indicates denser materials.

2.1. Sediment Dating and Age Model

Sediment dating was performed using both ^{210}Pb (T1/2 = 22.3 years) along the upper 19 cm of the core and AMS (Accelerator Mass Spectrometry) radiocarbon ^{14}C dating performed at the bottom of the core at 21–22 cm bsf.

Modern sediment accumulation rates (SARs) were determined from the activity–depth profile of the excess ^{210}Pb. The total and supported ^{210}Pb activities were measured using gamma spectroscopy with high-purity coaxial germanium detector Canberra GX2520 at the Institute of Geology, Adam Mickiewicz University in Poznań (Poland). For this analysis, the samples were dried, homogenised, packeted, and sealed, then left for at least 21 days prior to measurements in order to re-equilibrate ^{210}Pb with its precursor ^{222}Rn before the following gamma counting of ^{226}Ra, ^{214}Bi, and ^{214}Pb. For the age and SAR calculations, the constant initial concentration (CIC) model was applied [23]. To avoid the impact of compaction on the age calculation, the sediment mass accumulation rate (MAR) was also calculated using the sediment's dry bulk density to calculate the mass depth (g cm^{-2}).

The base of the core, at 21–22 cm bsf, was dated with AMS C^{14} radiocarbon dating at the NOSAMS Laboratory (Woods Hole, MA, USA) using a monospecific sample of *Neogloboquadrina pachyderma* tests. The raw ^{14}C data (765 ± 15 years) were calibrated with CALIB software version 8.2 [24], using the Marine20 calibration curve [25], applying a global ocean reservoir correction (R) of 400 years and an average marine regional reservoir effect of delta R = 76 ± 26 years to accommodate local effects in the Svalbard area, as indicated by Mangerud et al. [26] and Bondevik et al. [27].

2.2. Geochemistry: X-ray Fluorescence (XRF) Core Scan Analysis

Continuous downcore XRF analysis on the box-core GS191-02BC was performed at a resolution of 1 cm using an Avaatech Superslit X-ray fluorescence core scan (XRF core scan) under the 10 kv and 30 kv instrumental settings at the ISMAR-CNR, Bologna (Italy). For this work, we considered the Zr/Rb ratio as a proxy of the sediment grain size, with high values indicating a higher content of coarse silt and sand fractions, e.g., ref. [28]; the Ca/Ti ratio as a proxy of the biogenic carbonate content, i.e., refs. [29,30]; and the Br/Ti ratio as a proxy of the biological paleoproductivity, i.e., refs. [31–33].

2.3. Micropaleontological Analysis

For the micropaleontological analysis, 0.5 cm (for the first 2 cm) and 1 cm thick sediment samples down to the core bottom were oven-dried, weighed, and wet-sieved with filtered tap water using a mesh size of 63 μm to eliminate the fine fraction. The sandy fraction (>63 μm) was dried for 24 h in an oven at 40 °C and weighed again. Then, the sand-sized fraction was dry-sieved at 150 μm.

For the micropaleontological analysis, we used the 150 μm sieved fraction, subdivided into equal amounts by a microsplitter until a statistically representative sub-portion was

obtained. At least 300 planktic and 300 benthic foraminifera specimens were dry picked and identified at the species level. The planktic foraminifera were classified following the taxonomy of Darling et al. [34], Hemleben et al. [35], and Altuna et al. [36]. The benthic specimens were identified at the species level, following the taxonomy of the Ellis and Messina catalogues [37], Loeblich and Tappan [38–40], Feyling–Hanssen et al. [41], Gabel [42], Knudsen [43], Wollenburg and Mackensen [44], Holbourn et al. [45], and Setoyama and Kaminski [46]. The foraminiferal data are expressed as the relative abundance (%) and flux (spec. cm^{-2} yr^{-1}), as the PFAR (Planktic Foraminiferal Accumulation Rate) and BFAR (Benthic Foraminiferal Accumulation Rate). We consider as main species those present in proportions of more than 5% in one or more samples. The paleoenvironmental significance of each species was established using the literature available for similar geographical areas (see Table 2). The diversity indexes (dominance D and Shannon index H) and cluster analysis were computed using the freely available software Paleontological Statistics PAST version 4.16c [47].

Table 2. Ecological characteristics of the dominant planktic and benthic foraminiferal species.

	Main Species	Environmental Conditions	Refs.
Planktic species	*Neogloboquadrina pachyderma* (Ehrenberg, 1861)	Polar species. Related to Arctic and polar surface waters.	[48–52]
	Neogloboquadrina incompta (Cifelli, 1961), *Globigerina bulloides* d'Orbigny, 1826, *Globigerinita glutinata* (Egger, 1893)	Subpolar species related to Atlantic water. Seasonal peak abundances in late summer.	[48,49,51,53,54]
	Turborotalita quinqueloba (Natland, 1938)	Subpolar species. Arctic water and related to the Arctic and polar fronts. Near-surface dweller. In areas influenced by warm Atlantic water.	[48,49,51–53,55]
Benthic species	*Cassidulina laevigata* d'Orbigny, 1826	Warm, high-salinity bottom water of Atlantic origin and sandy substrates.	[56,57]
	Cassidulina neoteretis Seidenkrantz, 1995	Cool transformed surface Atlantic water. Stable salinity. Seasonal ice-free conditions. High seasonal productivity. Warm bottom conditions. Epifaunal–shallow infaunal species.	[44,57–62]
	Cassidulina reniforme Nørvang, 1945	Arctic–polar species. Cold and salty. Locally related to glaciomarine environments. Associated with *E. clavatum*. Epifaunal–shallow infaunal.	[63–68]
	Cibicidoides wuellerstorfi (Schwager, 1866)	Associated with Arctic waters and Arctic/polar fronts. High-energy environments. Bottom current activity. Epifaunal in coarser sediments and attached to hard substrates.	[44,63,64,69,70]
	Epistominella exigua (Brady, 1884)	Opportunistic species, feeds on fresh phytodetritus. Epifaunal.	[44,71,72]
	Oridorsalis tener (Brady, 1884)	Related to low productivity. Deep water species, 2000–3000 m	[44,73]

3. Results

3.1. Chronology and Sedimentation Rate

The age model was primarily developed using the excess ^{210}Pb profile on the upper 19 cm of the core, and the results were then compared to the radiocarbon ^{14}C dating results of one sample collected at the bottom of the core (21–22 cm bsf). According to the excess ^{210}Pb profile, the deeper measured interval at 18–19 cm bsf has an estimated age of 1890 ± 25 y AD, with a sediment accumulation rate in the core of 0.148 cm y^{-1} (Table S1). This value is in accordance with the ^{14}C radiocarbon date of 1550–1703 Cal y (1-sigma, 1640 Cal y with median probability) obtained at the bottom of the core.

3.2. Geochemistry

The profile of the Zr/Rb ratio indicates an initial interval located between the base of the core and 10.5 cm bsf (1890–1944 AD) characterised by an almost stable trend, followed by a progressive coarsening upward to the top of the core (Figure 3). The more consistent increase in the uppermost 5 cm corresponds with the presence of sparse IRD and abundant bioclasts, visible in the radiography as white dots and observed during the micropaleontological analysis. The Br/Ti ratio outlines three main intervals of possible higher productivity located within 1915–1930 AD (14–12.5 cm bsf), at around 1955 AD (8 cm bsf), and in the interval younger than 1990 AD (uppermost 5 cm of the core). The Ca/Ti ratio progressively increases upcore, having a more consistent increase between 1970 and 1990 AD. Minimum values were recorded at the base of the core (1896 AD) and at 12 cm bsf, corresponding to 1937 AD (Figure 3).

3.3. Planktic Foraminifera

Six planktic foraminiferal species were recognised, and five of them were present in proportions of more than 5% in one or more levels: *Globigerina bulloides*, *Globigerinita glutinata*, *Neogloboquadrina incompta*, *Neogloboquadrina pachyderma*, *Turborotalita quinqueloba*, and *Globigerinita uvula* (Figure 4). The total planktic foraminiferal flux (PFAR) shows an upward decreasing trend, varying from a maximum of ca. 200 spec. cm^{-2} yr^{-1} at 1903 AD to a minimum of 25 spec. cm^{-2} yr^{-1} at ca. 2014 AD (Figure 4).

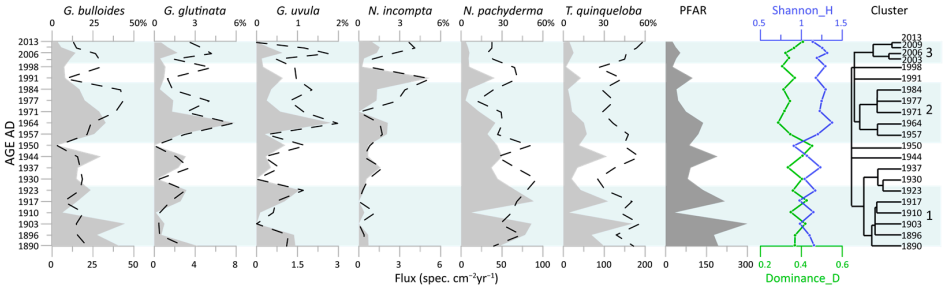

Figure 4. Planktic foraminiferal species vs. age: Dashed black line: percentage of relative abundance of each planktic foraminifera species; Light-grey area: flux of planktic foraminiferal species; Dark-grey area: Planktic Foraminiferal Accumulation Rate (PFAR); Shannon index (blue line) and Dominance (green line) of the planktic foraminiferal assemblages; Stratigraphically constrained cluster analysis of the planktic foraminifera, distinguished from 1 to 3 by light blue areas.

The diversity indexes are very constant along the whole sediment record, due to the low number of planktic species, although a prominent change occurs in the record after 1950 AD (Figure 4).

The stratigraphically constrained cluster analysis allowed us to define three planktic foraminiferal clusters, called 1 to 3 from the bottom to the top of the core, and four outliers corresponding to the years 1944, 1950, 1991, and 1998 (Figure 4). The first planktic foraminiferal cluster (cluster 1) ranges from ca. 1890 to 1940 AD and is dominated by a high relative abundance of *N. pachyderma* and *T. quinqueloba*, reaching 55% at ca. 1930 AD and 56% at ca. 1954 AD, respectively. The highest value of PFAR took place during this time interval, together with the maximum flux of *G. bulloides* at ca. 1903 AD with 44 spec. cm^{-2} yr^{-1}.

The period from ca. 1941 to 1953 AD, which cannot fit in any cluster, is characterised by a high variability in the relative abundances of *T. quinqueloba* (56% at ca. 1944 AD) and of *N. pachyderma* (from 26% to 51%), with *G. bulloides* reaching the minimum relative abundance of 3%.

The planktic foraminiferal assemblage of cluster 2 (from ca. 1954 to 1987 AD) is characterised by a high percentage of *G. bulloides* with values ranging from 21% to 43%. *Globigerinita glutinata* and *G. uvula* also have their highest abundance during this period, whereas the Neogloboquadrinids show the lowest abundance (Figure 4).

The samples recording the period from ca. 1988 to 2000 AD, corresponding to the four outliers of the cluster analysis, show high variability in the foraminiferal relative abundances of *N. incompta* (5–39%), *T. quinqueloba* (43–26%), and *G. bulloides* (8–29%), whereas *N. pachyderma* maintains constant values (Figure 4). The foraminiferal assemblage in cluster 3 (from ca. 2001 to 2013 AD) is characterised by a relatively high abundance of *T. quinqueloba*, with a maximum of 58% at ca. 2013 AD, and a relatively constant trend for *N. pachyderma*, ranging between 23 and 19% (Figure 4).

3.4. Benthic Foraminifera

Seventy-one benthic foraminiferal taxa were identified, and twelve of them were main species. These included seven calcareous perforate taxa (*Cassidulina laevigata*, *Cassidulina neoteretis*, *Cassidulina reniforme*, *Cibicidoides wuellerstorfi*, *Epistominella exigua*, *Oridorsalis tener*, and *Parrelloides* cf. *healdi*) and five agglutinated taxa (*Adercotryma* cf. *glomeratum*, *Labrospira crassimargo*, *Labrospira subglobosa*, *Recurvoides trochamminiforme*, and *Reophax scorpiurus*) (Figure 5). The secondary species were present in proportions of less than 5% (see Supplementary Materials Table S2 and Figure S1). The BFAR reached a maximum of 141 spec. cm^{-2} yr^{-1} at ca. 1923 AD and a minimum value at ca. 1910 AD, with 17 spec. cm^{-2} yr^{-1} (Figure 5). The Shannon index (H) shows its maximum values (up to 2.73 at ca. 1937 AD) in the bottom part of the record, decreasing to a minimum value of 2.13 at ca. 1971 AD. From 1971 AD to 1987 AD, the Shannon index has high values (2.48), decreasing toward the top of the core. The dominance (D) slightly increases from ca. 1950 AD until ca. 1980 AD, reaching its maximum value of 0.225. Then, the D record becomes relatively stable, ranging between a minimum of 0.112 at ca. 1984 AD and a maximum of 0.197 at ca. 2003 AD (Figure 5).

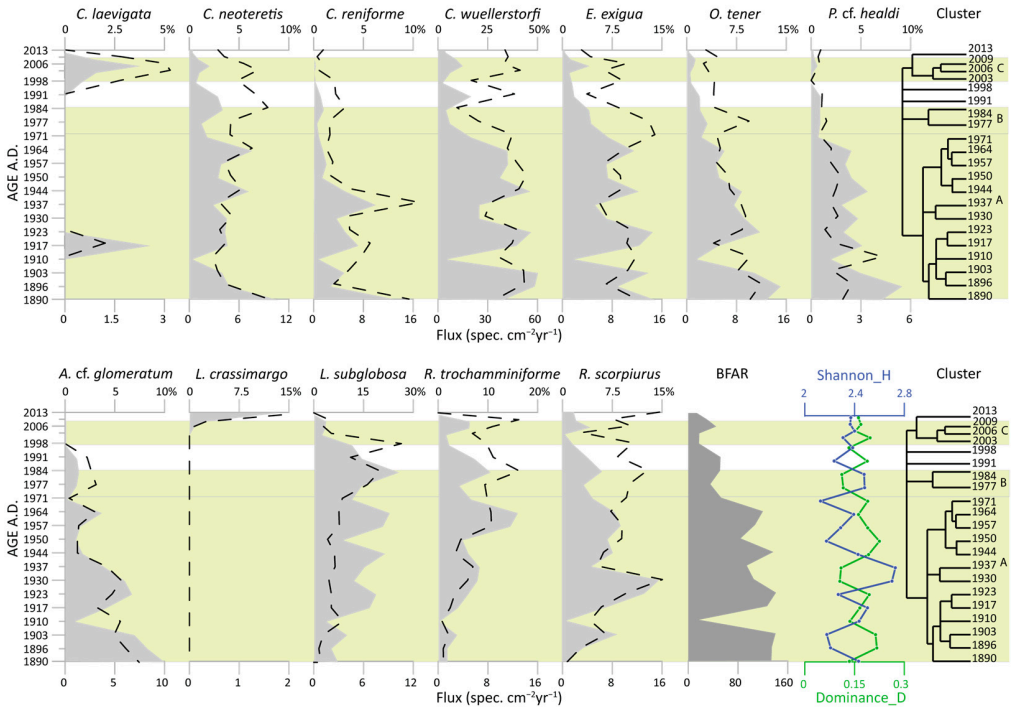

Figure 5. Benthic foraminiferal species percentages vs. age. Dashed black line: percentage of relative abundance of benthic foraminiferal species; Light-grey area: flux of benthic foraminiferal species; Dark-grey area: Benthic Foraminiferal Accumulation Rate (BFAR); Shannon index (blue line) and Dominance (green line) of the benthic foraminiferal assemblages; Stratigraphically constrained cluster analysis of the benthic foraminifera, distinguished from A to C and highlighted by lime-yellow areas.

The stratigraphically constrained cluster analysis indicates three clusters of benthic foraminiferal assemblages, which were identified as A to C, with three outliers (Figure 5).

The first benthic foraminiferal assemblage, cluster A (from ca. 1890 AD to 1974 AD), shows a generally high relative abundance of the main species: *C. wuellerstorfi*, reaching a maximum of 44% at ca. 1950 AD; *E. exigua* (6–14%); *C. reniforme* (1–11%); *C. neoteretis* (2–8%); and *O. tener* (10–5%). The relative percentages of the agglutinated species *R. trochamminiforme* and *L. subglobosa* vary from 1 to 9% and from 2 to 10%, respectively, and *R. scorpiurus* displays a variable trend, reaching 15% at ca. 1937 AD. The BFAR is characterised by high values, except for a major decrease at ca. 1917 AD.

The foraminiferal assemblage of cluster B (from ca. 1975 AD to ca. 1987 AD) reveals a decreasing trend for *C. wuellerstorfi*, *E. exigua*, and *O. tener*, with ranges of 20 to 9%, 13 to 8%, and 9 to 4%, respectively, whereas a consistent increase was observed for the agglutinated foraminifera *L. subglobosa* (16 to 20%), *R. trochamminiforme* (9 to 16%), and *R. scorpiurus* (10 to 13%) (Figure 6). The BFAR is generally characterised by low values (35–51 spec. cm^{-2} yr^{-1}).

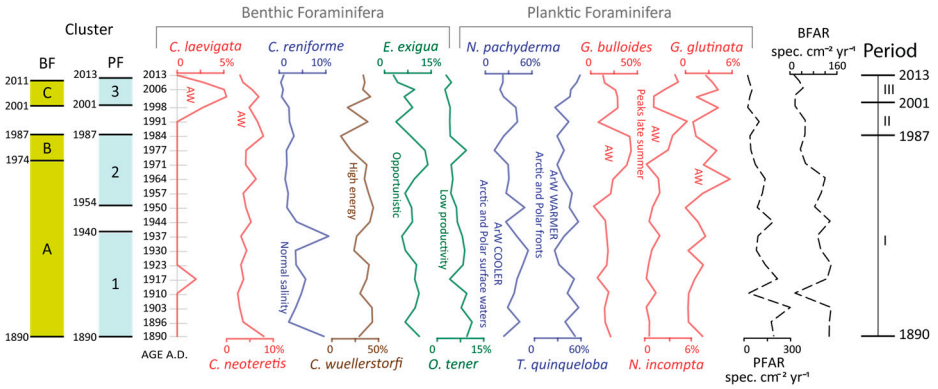

Figure 6. Main benthic and planktic foraminifera species with indications of their ecological significance. The graphics are colour-coded to represent different types of marine species: AW affinity (red), ArW affinity (blue), productivity-related (green), and current-energy-related (brown) species (for more information about the ecology of the species, refer to the main text and Table 2). The PFAR and BFAR are represented with dashed black lines. On the left, cluster divisions are represented with lime-yellow areas for the benthic foraminiferal clusters and baby-blue areas for the planktic foraminiferal clusters. On the right is the division of the three main climatic periods, as discussed in the main text.

According to the cluster analysis, the period from ca. 1988 to 2000 AD is characterised by a high variability in the relative abundance of *C. wuellerstorfi* (17–38%), a peak of 7% for *C. neoteretis*, and an increase in agglutinated species, such as *L. subglobosa* (11%) and *R. trochamminiforme* (8%).

The foraminiferal assemblage in cluster C (from ca. 2001 to ca. 2011 AD) is characterised by the occurrence of *C. laevigata* and high percentages of *C. wuellerstorfi*, reaching 41%, and *E. exigua* (10%). *Cassidulina reniformis* and some agglutinated species, such as *L. subglobosa*, *A.* cf. *glomeratum*, and *P.* cf. *healdi*, strongly decreased. The last recorded period (from ca. 2012 to ca. 2013 AD, identified as an outlier by the cluster analysis) is characterised by a lower presence of *C. wuellerstorfi*, at 34%; a strong decrease in *E. exigua* and *C. neoteretis*; and the appearance of the agglutinated species *L. crassimargo*.

4. Discussion

The sediment record collected in the Bellsund Drift allowed us to recognise some important oceanographic changes that were identified in both the planktic and benthic foraminiferal assemblages, together with geochemical indicators. The planktic assemblages reflect the surface and subsurface hydrographic changes that are often diachronous with respect to the changes occurring in the benthic assemblages. The latter reflect the evolution of the bottom water masses, but they are also strongly influenced by the flux of the organic matter derived from the primary productivity of surface waters.

The planktic–benthic decoupling is clearly depicted by the results of the two-cluster analysis performed on the planktic and benthic foraminifera assemblages, which have clusters separated by different stratigraphic boundaries. In the following paragraphs, we discuss the evolution of surface and deep-water masses since 1890 AD considering three main periods: 1890–1987 AD, 1987–2001 AD, and 2001–2013 AD (Figure 6).

The first period (1890 to 1987 AD) is a century characterised by generally cold conditions, interrupted by an event, between ca. 1940 and 1954 AD, characterised by milder conditions reflected only in the surface water masses. For ca. 1890–1940 AD, the dominance of *N. pachyderma* in the planktic assemblage indicates the prevalence of cold surface conditions. Divine and Dick [18] reported an expanded winter ice edge in the Fram Strait during the same period that was determined by cold winters. The cold conditions are also recorded in our dataset by the low abundance of the subpolar species *T. quinqueloba*, *N. incompta*, *G. bulloides*, and *G. glutinata*, which can be related to an increase in the influx of cold ArW in the region, as mentioned by Vinje [17]. The sea-bottom environment during ca. 1890–1974 AD was characterised by cold, oligotrophic, and high-energy conditions, indicated by the respective occurrence of *C. reniforme* and *O. tener* and the high abundance of *C. wuellerstorfi* [74]. The presence of a high-energy environment is also supported by the presence of relatively coarse-grained sediments, as indicated by the increase in the Zr/Rb ratio (proxy of grain size), suggesting an intensification of the bottom currents that could be related to enhanced deep convection.

A brief event characterised by warmer conditions was recorded between ca. 1940 and 1954 AD, and it was related to the influx of warm AW arriving from the Norwegian Sea [4,19,48,53]. The warmer conditions of the surface water led to an increase in the primary productivity and determined a high flux of planktic foraminifera, as also indicated in [48] and [75]. In our record, the increase in PFAR is linked to an increase in subpolar species *N. incompta*, *G. bulloides*, *G. glutinata*, and *T. quinqueloba* [55] (Table 2 and Figure 6) and an increase in the Br/Ti ratio (proxy of primary productivity). Werner et al. [4] argued that the contemporaneous high abundance of both ArW and AW species is associated with a warmer temperature of the upper part of the water column, associated with an increased inflow of AW, suggesting water mass stratification. The same authors suggested that this strong stratification in the water column was a common hydrographic structure during the 20th century.

The last part of the first period, ca. 1954–1987 AD, indicated cooler conditions in the surface water masses, inferred from the increase in the ArW indicator species *T. quinqueloba*, but also from the presence of the AW indicators *G. bulloides*, *G. glutinata*, and *N. incompta*. This cooler period has also been reported by several authors, e.g., refs. [17,76–78], who, on the basis of the planktic foraminiferal assemblage, hypothesised a raised temperature of the WSC transporting AW. Dickson et al. [79] and Spielhagen et al. [19] reported an increase in warm water planktic species occurring since ca. 1980 AD, confirming the spreading of AW into the Arctic Ocean. At the end of this phase, between ca. 1975 and 1987 AD, the studied area was influenced by a strong intensification of the AW, which previously influenced the upper water column and then deepened, reaching the sea bottom, as indicated by the higher abundance of the benthic foraminifera *C. neoteretis*. The warmer conditions created a stronger temperature gradient in the (sub)surface waters and improved the seasonal food supply, as indicated by the increase in the opportunistic taxon *E. exigua*, the presence of *C. neoteretis* and the agglutinated foraminifera, and the low abundance of *C. reniforme*. The decline of *C. wuellerstorfi* and the lower Zr/Rb ratio indicate a lower energy of the bottom currents. The high variety of benthic species, including the agglutinated foraminifera, indicates the presence of an organic-rich substrate supporting a high diversity of the benthic foraminifera populations [80].

The second period (1987–2001 AD) is characterised by generally warm conditions giving way to a stronger influence of warm waters, supported by the proliferation of warm species and by increasing diversification of the benthic foraminiferal assemblages. A cold spell influencing the surface water column is hypothesised to have occurred at the

beginning of the 1990s, identified by the increase in the cold planktic species *N. pachyderma*, the increase in the benthic foraminifera *C. wuellerstorfi*, and a coarser grain size (Zr/Rb ratio), all suggesting an intensification of the bottom current (Figure 3). This event was correlated with the cold event indicated to occur during the late 1980s by Divine and Dick [18]. A further rise in temperature was recorded between ca. 1995 AD and ca. 2000 AD, with the proliferation of *G. bulloides* and *G. glutinata* (Table 2 and Figure 6). This general warmer trend is in agreement with the warming trend dated ca. 1970-2008 AD recorded in the Arctic area [81]. This event was also documented by Quadfasel et al. [82], which, in turn, agreed with a study by Kinnard et al. [11] that indicated that a warm-water inflow in the Arctic Ocean started during the 1990s, producing heat conditions affecting the entire water column [6,79,83]. In the studied core, this warming trend was also recorded at the sea bottom from ca. 1988 to 1994 AD, with a high abundance of *C. neoteretis* and *C. laevigata* suggesting a continuous increasing influx of AW (Table 2 and Figure 6).

The last period, from ca. 2001 to 2013 AD, corresponds to a high-productivity phase that probably started at the end of the 1990s, indicated by the relatively high abundance of *T. quinqueloba* and the consistent presence of *N. pachyderma* [48,84] (Table 2 and Figure 6). The high organic flux to the sea bottom is supported by the presence of *E. exigua*, a phytodetritivorous species that proliferates when a pulse of labile organic matter reaches the sea floor. The satellite monitoring indicated a persistent warmer trend of the WSC, with progressive retreat of the sea ice in the northern area (Figure 2), producing a shortening of the winter periods and a decrease in seasonal sea ice. The planktic foraminiferal assemblages reflect these conditions in the sea surface water with increasing abundance of the warmer indicator species, such as *T. quinqueloba*, *N. incompta*, *G. glutinata*, and *G. bulloides* (Table 2). A general decreasing trend in the occurrence of the cool-water indicator *N. pachyderma* confirms the decrease in cold-water influx. Instead, the increase in the heat influx into the water column is associated with a strong reduction in the sea ice extent [21] and is depicted in the studied core by an increase in *C. laevigata* and *C. neoteretis* (Table 2 and Figure 6) with a stronger input of warm bottom currents through the WSC, depicted by the consistent presence of *C. wuellerstorfi* in coarse-grained sediments (high Zr/Rb ratio) (Table 2 and Figure 6). According to Kaufman et al. [85], the period within ca. 1999–2008 AD was the warmest of the last 200 years.

5. Conclusions

The sedimentary record of box-core GS191-02BC documents the past 120 years of the paleoceanographic history in the area of the Bellsund Drift, located south of the Fram Strait. The high-resolution analyses of the benthic and planktic foraminiferal assemblages allowed us to produce new insights into the recent and modern oceanic configuration in association with the climatic variability of the North Atlantic Ocean at the gate to the Arctic Ocean.

Three oceanographic periods were identified, outlining an overall warming trend.

The first period (ca. 1890–1987 AD) was characterised by consistently cold surface and bottom water masses, occasionally punctuated by brief intervals of warmer surface waters associated with Atlantic Water input.

The second period (ca. 1987–2001 AD) was characterised by warm surface and cold bottom water masses, with incursions of cold Arctic surface waters.

The third period (ca. 2001–2013 AD) was characterised by warm surface and bottom water masses clearly associated with a consistent inflow of Atlantic water.

The environmental reconstruction covering the past 120 years highlighted the amplified heat influx into the Arctic Ocean as an effect of the documented increasing inflow of Atlantic water (*Arctic Atlantification*), impacting the sea ice formation and distribution, with a strong effect on the oceanographic structure and climate.

Supplementary Materials: The following supporting information can be downloaded at: https://www.mdpi.com/article/10.3390/jmse12040559/s1, Table S1: Samples analysed for ^{210}Pb analysis and estimated age (AD). Table S2: Benthic foraminiferal taxa with relative abundance <5%. Figure S1: Benthic foraminiferal taxa with relative abundance <5% on the total benthic assemblage.

Author Contributions: C.M. and R.G.L. conceived and designed the research. R.G.L. directed the data acquisition during the EUROFLEETS-2 Cruise PREPARED and contributed to the sedimentological data interpretation. L.L. and R.G.L. defined the age model and sedimentation rate. V.M.G.S. processed and analysed the foraminiferal assemblage, combined the micropaleontological and sedimentological datasets, and led the writing of the manuscript. C.M. supervised the micropaleontological work, the data interpretation, and the writing of the manuscript. All authors have read and agreed to the published version of the manuscript.

Funding: Data acquisition for this research was supported by the European research infrastructure EUROFLEETS funding the project PREPARED (grant agreement n. 312762). Digital X-radiography was performed at ENI laboratories, and initial data analyses on the sediment cores (XRF core scan, digital photo, grain size) were supported by the Spanish project DEGLABAR (CTM2010-17386) and the Italian project CORIBAR-IT (PdR 2013/C2.01) funded by PNRA.

Institutional Review Board Statement: Not applicable.

Informed Consent Statement: Not applicable.

Data Availability Statement: The data that support the findings of this study are available from the corresponding authors, C.M. and V.M.G.S., upon reasonable request.

Acknowledgments: We thank the participants and crew on the EUROFLEETS-2 Cruise PREPARED on the R/V G.O. Sars. We especially thank Captain John Hugo Johnson, the officers, and the crew of Expedition 191 and the technicians Martin Dahl, Ingve Fjelstad, Dag Inge Blindheim, and Åse Sudman for their strong support during the acquisition activities.

Conflicts of Interest: The authors declare no conflicts of interest.

References

1. Rebesco, M.; Wåhlin, A.; Laberg, J.S.; Schauer, U.; Beszczynska-Möller, A.; Lucchi, R.G.; Noormets, R.; Accettella, D.; Zarayskaya, Y.; Diviacco, P. Quaternary contourite drifts of the Western Spitsbergen margin. *Deep Sea Res. Part I Oceanogr. Res. Pap.* **2013**, *79*, 156–168. [CrossRef]
2. Werner, A. Holocene moraine chronology, Spitsbergen, Svalbard: Lichenometric evidence for multiple Neoglacial advances in the Arctic. *Holocene* **1993**, *3*, 128–137. [CrossRef]
3. Svendsen, J.I.; Mangerud, J. Holocene glacial and climatic variations on Spitsbergen, Svalbard. *Holocene* **1997**, *7*, 45–57. [CrossRef]
4. Werner, K.; Spielhagen, R.F.; Bauch, D.; Hass, H.C.; Kandiano, E.; Zamelczyk, K. Atlantic Water advection to the eastern Fram Strait—Multiproxy evidence for late Holocene variability. *Palaeogeogr. Palaeoclimatol. Palaeoecol.* **2011**, *308*, 264–276. [CrossRef]
5. Quadfasel, D.; Rudels, B.; Kurz, K. Outflow of dense water from a Svalbard fjord into the Fram Strait. *Deep Sea Res. Part A Oceanogr. Res. Pap.* **1988**, *35*, 1143–1150. [CrossRef]
6. Nilsen, F.; Skogseth, R.; Vaardal-Lunde, J.; Inall, M. A simple shelf circulation model: Intrusion of Atlantic Water on the West Spitsbergen Shelf. *J. Phys. Oceanogr.* **2016**, *46*, 1209–1230. [CrossRef]
7. Langehaug, H.R.; Falck, E. Changes in the properties and distribution of the intermediate and deep waters in the Fram Strait. *Prog. Oceanogr.* **2012**, *96*, 57–76. [CrossRef]
8. Rudels, B.; Friedrich, H.J.; Quadfasel, D. The Arctic circumpolar boundary current. *Deep Sea Res. Part II Top. Stud. Oceanogr.* **1999**, *46*, 1023–1062. [CrossRef]
9. Karcher, M.J.; Gerdes, R.; Kauker, F.; Köberle, C. Arctic warming: Evolution and spreading of the 1990s warm event in the Nordic seas and the Arctic Ocean. *J. Geophys. Res. Ocean.* **2003**, *108*, 1–16. [CrossRef]
10. Schauer, U.; Fahrbach, E.; Osterhus, S.; Rohardt, G. Arctic warming through the Fram Strait: Oceanic heat transport from 3 years of measurements. *J. Geophys. Res. Ocean.* **2004**, *109*, C06026. [CrossRef]
11. Kinnard, C.; Zdanowicz, C.M.; Fisher, D.A.; Isaksson, E.; de Vernal, A.; Thompson, L.G. Reconstructed changes in Arctic Sea ice over the past 1,450 years. *Nature* **2011**, *479*, 509–512. [CrossRef]
12. Müller, J.; Werner, K.; Stein, R.; Fahl, K.; Moros, M.; Jansen, E. Holocene cooling culminates in sea ice oscillations in Fram Strait. *Quat. Sci. Rev.* **2012**, *47*, 1–14. [CrossRef]
13. Wang, Q.; Wekerle, C.; Wang, X.; Danilov, S.; Koldunov, N.; Sein, D.; Sidorenko, D.; von Appen, W.J.; Jung, T. Intensification of the Atlantic Water supply to the Arctic Ocean through Fram Strait induced by Arctic Sea ice decline. *Geophys. Res. Lett.* **2020**, *47*, e2019GL086682. [CrossRef]
14. Tuerena, R.E.; Hopkins, J.; Buchanan, P.J.; Ganeshram, R.S.; Norman, L.; von Appen, W.J.; Tagliabue, A.; Doncila, A.; Graeve, M.; Ludwichowski, K.U.; et al. An Arctic strait of two halves: The changing dynamics of nutrient uptake and limitation across the Fram Strait. *Global Biogeochem. Cycles* **2021**, *35*, e2021GB006961. [CrossRef]
15. Hofmann, Z.; von Appen, W.J.; Wekerle, C. Seasonal and mesoscale variability of the two Atlantic Water recirculation pathways in Fram Strait. *J. Geophys. Res. Oceans* **2021**, *126*, e2020JC017057. [CrossRef]

16. Ślubowska, M.A.; Koç, N.; Rasmussen, T.L.; Klitgaard-Kristensen, D. Changes in the flow of Atlantic water into the Arctic Ocean since the last deglaciation: Evidence from the northern Svalbard continental margin, 80 °N. *Paleoceanography* **2005**, *20*, PA4014. [CrossRef]
17. Vinje, T. Anomalies and trends of sea-ice extent and atmospheric circulation in the Nordic Seas during the period 1864–1998. *J. Clim.* **2001**, *14*, 255–267. [CrossRef]
18. Divine, D.V.; Dick, C. Historical variability of sea ice edge position in the Nordic Seas. *J. Geophys. Res. Ocean.* **2006**, *111*, 1–14. [CrossRef]
19. Spielhagen, R.F.; Werner, K.; Sørensen, S.A.; Zamelczyk, K.; Kandiano, E.; Budeus, G.; Husum, K.; Marchitto, T.M.; Hald, M. Enhanced modern heat transfer to the Arctic by warm Atlantic water. *Science* **2011**, *331*, 450–453. [CrossRef]
20. Tesi, T.; Muschitiello, F.; Mollenhauer, G.; Miserocchi, S.; Langone, L.; Ceccarelli, C.; Panieri, G.; Chiggiato, J.; Nogarotto, A.; Hefter, J.; et al. Rapid Atlantification along the Fram Strait at the beginning of the 20th century. *Sci. Adv.* **2021**, *7*, eabj2946. [CrossRef]
21. Comiso, J.C.; Parkinson, C.L.; Gersten, R.; Stock, L. Accelerated decline in the Arctic Sea ice cover. *Geophys. Res. Lett.* **2008**, *35*, L01703. [CrossRef]
22. Lucchi, R.G.; Kovacevic, V.; Aliani, S.; Caburlotto, A.; Celussi, M.; Corgnati, L.; Cosoli, S.; Deponte, D.; Ersdal, E.A.; Fredriksson, S.; et al. *PREPARED: Present and Past Flow Regime on Contourite Drifts West of Spitsbergen*; EUROFLEETS-2 Cruise Summary Report, R/V G.O. Sars Cruise No. 191, 05/06/2014–15/06/2014; Tromsø, Norway, 2014; p. 89. Available online: https://www.researchgate.net/publication/266556598_PREPARED_Present_and_past_flow_regime_On_contourite_drifts_west_of_Spitsbergen (accessed on 18 March 2024). [CrossRef]
23. Kirchner, G. ^{210}Pb as a tool for establishing sediment chronologies: Examples of potentials and limitations of conventional dating models. *J. Enviro. Radioact.* **2011**, *102*, 490–494. [CrossRef] [PubMed]
24. Stuiver, M.; Reimer, P.J. Extended ^{14}C data base and revised CALIB 3.0 ^{14}C age calibration program. *Radiocarbon* **1993**, *35*, 215–230. [CrossRef]
25. Heaton, T.J.; Köhler, P.; Butzin, M.; Bard, E.; Reimer, R.W.; Austin, W.E.N.; Bronk Ramsey, C.; Hughen, K.A.; Kromer, B.; Reimer, P.J.; et al. Marine20-the marine radiocarbon age calibration curve (0–55,000 cal BP). *Radiocarbon* **2020**, *62*, 779–820. [CrossRef]
26. Mangerud, J.; Bondevik, S.; Gulliksen, S.; Hufthammerd, A.K.; Høisætere, T. Marine ^{14}C reservoir ages for 19th century whales and molluscs from the North Atlantic. *Quat. Sci. Rev.* **2006**, *25*, 23–24, 3228–3245. [CrossRef]
27. Bondevik, S.; Mangerud, J.; Birks, H.H.; Gulliksen, S.; Reimer, P. Changes in North Atlantic radiocarbon reservoir ages during the Allerød and Younger Dryas. *Science* **2006**, *312*, 1514–1517. [CrossRef]
28. Wu, L.; Wilson, D.J.; Wang, R.; Yin, X.; Chen, Z.; Xiao, W.; Huang, M. Evaluating Zr/Rb ratio from XRF scanning as an indicator of grain-size variations of glaciomarine sediments in the Southern Ocean. *Geochem. Geophys. Geosyst.* **2020**, *21*, e2020GC009350. [CrossRef]
29. Olsen, J.; Anderson, N.J.; Knudsen, M.F. Variability of the North Atlantic Oscillation over the past 5200 years. *Nat. Geosci.* **2012**, *5*, 808–812. [CrossRef]
30. Lucchi, R.G.; Camerlenghi, A.; Rebesco, M.; Colmenero-Hidalgo, E.; Sierro, F.J.; Sagnotti, L.; Giorgetti, G. Postglacial sedimentary processes on the Storfjorden and Kveithola trough mouth fans: Significance of extreme glacimarine sedimentation. *Glob. Planet Change* **2013**, *111*, 309–326. [CrossRef]
31. Thomson, J.; Croudace, I.W.; Rothwell, R.G. A geochemical application of the ITRAX scanner to a sediment core containing eastern Mediterranean sapropel units. In: Rothwell RG (ed) New Techniques in Sediment Core Analysis. *Geol. Soc. Spec. Publ.* **2006**, *267*, 65–77. [CrossRef]
32. Itambi, A.C.; Von Dobeneck, T.; Adegbie, A.T. Millennial-scale precipitation changes over Central Africa during the late Quaternary and Holocene: Evidence in sediments from the Gulf of Guinea. *J. Quat. Sci.* **2010**, *25*, 267–279. [CrossRef]
33. Caley, T.; Malaizé, B.; Zaragosi, S.; Rossignol, L.; Bourget, J.; Eynaud, F.; Martinez, P.; Giraudeau, J.; Charlier, K.; Ellouz-Zimmermann, N. New Arabian Sea records help decipher orbital timing of Indo-Asian monsoon. *Earth Planet. Sci. Lett.* **2011**, *308*, 433–444. [CrossRef]
34. Darling, K.F.; Kucera, M.; Kroon, D.; Wade, C.M. A resolution for the coiling direction paradox in *Neogloboquadrina pachyderma*. *Paleoceanography* **2006**, *21*, 1–14. [CrossRef]
35. Hemleben, C.; Spindler, M.; Anderson, O.R. *Modern Planktonic Foraminifera*; Springer Science Business Media: New York, NY, USA, 2012; pp. 1–362.
36. Altuna, N.E.B.; Pieńkowski, A.J.; Eynaud, F.; Thiessen, R. The morphotypes of *Neogloboquadrina pachyderma*: Isotopic signature and distribution patterns in the Canadian Arctic Archipelago and adjacent regions. *Mar. Micropaleontol.* **2018**, *142*, 13–24. [CrossRef]
37. Ellis, B.E.; Messina, A.R. *Catalogue of Foraminifera American Museum of Natural History*; Special Publications: New York, NY, USA, 1940.
38. Loeblich, A.R.; Tappan, H.N. Studies of Arctic foraminifera. *Smithson. Misc. Collect.* **1953**, *121*, 7.
39. Loeblich, A.R.; Tappan, H. *Foraminiferal Genera and Their Classification*; Van Nostrand Reinhold Co.: New York, NY, USA, 1987; pp. 1–2114.
40. Loeblich, A.R., Jr.; Tappan, H. *Foraminiferal Genera and Their Classification*; Springer: New York, NY, USA, 2015; pp. 1–846.
41. Feyling-Hanssen, R.W.; Jørgensen, J.A.; Knudsen, K.L.; Lykke-Andersen, A.L. Late Quaternary Foraminifera from Vendsyssel, Denmark and Sandnes, Norway. *Bull. Geol. Soc. Den.* **1971**, *21*, 67–317.

42. Gabel, B. Die Foraminiferen der Nordsee. *Helgoländer Wiss. Meeresunters.* **1971**, *22*, 1–65. [CrossRef]
43. Knudsen, K.L. Foraminiferer i Kvartær stratigrafi: Laboratorie-og fremstillingsteknik samt udvalgte eksempler. *Geol. Tidsskr.* **1998**, *3*, 1–25.
44. Wollenburg, J.E.; Mackensen, A. Living benthic foraminifers from the central Arctic Ocean: Faunal composition, standing stock and diversity. *Mar. Micropaleontol.* **1998**, *34*, 153–185. [CrossRef]
45. Holbourn, A.; Henderson, A.S.; MacLeod, N. *Atlas of Benthic Foraminifera*; John Wiley & Sons, Ltd.: Hoboken, NJ, USA; London, UK, 2013; Volume 654, pp. 1–656.
46. Setoyama, E.; Kaminski, M.A. Neogene benthic foraminifera from the southern Bering Sea (IODP Expedition 323). *Palaeontol. Electron.* **2015**, *18*, 1–30. Available online: https://palaeo-electronica.org/content/2015/1264-bering-benthic-forams (accessed on 18 March 2024). [CrossRef]
47. Hammer, Ø.; Harper, D.A.T.; Ryan, P.D. PAST: Paleontological statistics software package for education and data analysis. *Palaeontol. Electron.* **2001**, *4*, 9. Available online: https://palaeo-electronica.org/2001_1/past/past.pdf (accessed on 18 March 2024).
48. Carstens, J.; Hebbeln, D.; Wefer, G. Distribution of planktic foraminifera at the ice margin in the Arctic (Fram Strait). *Mar. Micropaleontol.* **1997**, *29*, 257–269. [CrossRef]
49. Bé, A.W.H.; Tolderlund, D.S. Distribution and Ecology of Living Planktonic Foraminifera in Surface Waters of the Atlantic and Indian Oceans. In *The Micropaleontology of the Oceans*; Funnell, B.M., Riedel, W.R., Eds.; Cambridge University Press: Cambridge, UK, 1971; pp. 105–149.
50. Kohfeld, K.E.; Fairbanks, R.G.; Smith, S.L.; Walsh, I.D. *Neogloboquadrina pachyderma* (sinistral coiling) as paleoceanographic tracers in polar oceans: Evidence from Northeast Water Polynya plankton tows, sediment traps, and surface sediments. *Paleoceanography* **1996**, *11*, 679–699. [CrossRef]
51. Simstich, J.; Sarnthein, M.; Erlenkeuser, H. Paired $\delta^{18}O$ signals of *Neogloboquadrina pachyderma*(s) and *Turborotalita quinqueloba* show thermal stratification structure in Nordic Seas. *Mar. Micropaleontol.* **2003**, *48*, 107–125. [CrossRef]
52. Schiebel, R.; Hemleben, C. Modern planktic foraminifera. *Paläontologische Z.* **2005**, *79*, 135–148. [CrossRef]
53. Volkmann, R. Planktic foraminifers in the outer Laptev Sea and the Fram Strait—Modern distribution and ecology. *J. Foraminifer. Res.* **2000**, *30*, 157–176. [CrossRef]
54. Schiebel, R.; Waniek, J.; Bork, M.; Hemleben, C. Planktic foraminiferal production stimulated by chlorophyll redistribution and entrainment of nutrients. *Deep Sea Res. Part I Oceanogr. Res. Pap.* **2001**, *48*, 721–740. [CrossRef]
55. Husum, K.; Hald, M. Arctic planktic foraminiferal assemblages: Implications for subsurface temperature reconstructions. *Mar. Micropaleontol.* **2012**, *96*, 38–47. [CrossRef]
56. Lagoe, M.B. Recent benthic foraminifera from the central Arctic Ocean. *J. Foraminifer. Res.* **1977**, *7*, 106–129. [CrossRef]
57. Mackensen, A.; Hald, M. *Cassidulina teretis* Tappan and *C. laevigata* d'Orbigny; their modern and late Quaternary distribution in northern seas. *J. Foraminifer. Res.* **1988**, *18*, 16–24. [CrossRef]
58. Lagoe, M.B. Recent benthonic foraminiferal biofacies in the Arctic Ocean. *Micropaleontology* **1979**, *25*, 214–224. [CrossRef]
59. Jennings, A.E.; Weiner, N.J. Environmental change in eastern Greenland during the last 1300 years: Evidence from foraminifera and lithofacies in Nansen Fjord, 68 N. *Holocene* **1996**, *6*, 179–191. [CrossRef]
60. Lubinski, D.J.; Polyak, L.; Forman, S.L. Freshwater and Atlantic water inflows to the deep northern Barents and Kara seas since ca 13 ^{14}C ka: Foraminifera and stable isotopes. *Quat. Sci. Rev.* **2001**, *20*, 1851–1879. [CrossRef]
61. Wollenburg, J.E.; Knies, J.; Mackensen, A. High-resolution paleoproductivity fluctuations during the past 24 kyr as indicated by benthic foraminifera in the marginal Arctic Ocean. *Palaeogeogr. Palaeoclimatol. Palaeoecol.* **2004**, *204*, 209–238. [CrossRef]
62. Jennings, A.E.; Weiner, N.J.; Helgadottir, G.; Andrews, J.T. Modern foraminiferal faunas of the southwestern to northern Iceland shelf: Oceanographic and environmental controls. *J. Foraminifer. Res.* **2004**, *34*, 180–207. [CrossRef]
63. Sejrup, H.P.; Fjaeran, T.; Hald, M.; Beck, L.; Hagen, J.; Miljeteig, I.; Morvik, I.; Norvik, O. Benthonic foraminifera in surface samples from the Norwegian continental margin between 62 degrees N and 65 degrees N. *J. Foraminifer. Res.* **1981**, *11*, 277–295. [CrossRef]
64. Mackensen, A.; Sejrup, H.P.; Jansen, E. The distribution of living benthic foraminifera on the continental slope and rise off southwest Norway. *Mar. Micropaleontol.* **1985**, *9*, 275–306. [CrossRef]
65. Hald, M.; Korsun, S. Distribution of modern benthic foraminifera from fjords of Svalbard, European Arctic. *J. Foraminifer. Res.* **1997**, *27*, 101–122. [CrossRef]
66. Korsun, S.; Hald, M. Seasonal dynamics of benthic foraminifera in a glacially fed fjord of Svalbard, European Arctic. *J. Foraminifer. Res.* **2000**, *30*, 251–271. [CrossRef]
67. Polyak, L.; Korsun, S.; Febo, L.A.; Stanovoy, V.; Khusid, T.; Hald, M.; Paulsen, B.E.; Lubinski, D.J. Benthic foraminiferal assemblages from the southern Kara Sea, a river-influenced Arctic marine environment. *J. Foraminifer. Res.* **2002**, *32*, 252–273. [CrossRef]
68. Steinsund, P.I.; Polyak, L.; Hald, M.; Mikhailov, V.; Korsun, S. Distribution of Calcareous Benthic Foraminifera in Recent Sediments of the Barents and Kara Sea. Benthic Foraminifera in Surface Sediments of the Barents and Kara Seas: Modern and Late Quaternary Application. Ph.D. Thesis, Department of Geology, Institute of Biology and Geology, University of Tromsø, Tromsø, Norway, 1994.
69. Belanger, P.E.; Streeter, S.S. Distribution and ecology of benthic foraminifera in the Norwegian-Greenland Sea. *Mar. Micropaleontol.* **1980**, *5*, 401–428. [CrossRef]

70. Bauch, H.A.; Erlenkeuser, H.; Spielhagen, R.F.; Struck, U.; Matthiessen, J.; Thiede, J.; Heinemeier, J. A multiproxy reconstruction of the evolution of deep and surface waters in the subarctic Nordic seas over the last 30,000 yr. *Quat. Sci. Rev.* **2001**, *20*, 659–678. [CrossRef]
71. Gooday, A.J. Deep-sea benthic foraminiferal species which exploit phytodetritus: Characteristic features and controls on distribution. *Mar. Micropaleontol.* **1993**, *22*, 187–205. [CrossRef]
72. Thomas, E.; Booth, L.; Maslin, M.; Shackleton, N.J. Northeastern Atlantic benthic foraminifera during the last 45,000 years: Changes in productivity seen from the bottom up. *Paleoceanography* **1995**, *10*, 545–562. [CrossRef]
73. Osterman, L.E.; Poore, R.Z.; Foley, K.M. *Distribution of Benthic Foraminifers (>125 mm) in the Surface Sediments of the Arctic Ocean*; Bulletin 2164; U. S. Geological Survey: Reston, VA, USA, 1999. [CrossRef]
74. Altenbach, A.V.; Sarnthein, M. Productivity Record in Benthic foraminifera. In *Productivity of the Ocean: Present and Past*; Berger, W.H., Smetacek, W.S., Wefer, G., Eds.; John Wiley and Sons: Berlin, Germany, 1989; pp. 8–255.
75. Pados, T.; Spielhagen, R.F. Species distribution and depth habitat of recent planktic foraminifera in Fram Strait, Arctic Ocean. *Polar Res.* **2014**, *33*, 22483. [CrossRef]
76. Polyakov, I.V.; Alekseev, G.V.; Timokhov, L.A.; Bhatt, U.S.; Colony, R.L.; Simmons, H.L.; Walsh, D.; Walsh, J.E.; Zakharov, V.F. Variability of the intermediate Atlantic water of the Arctic Ocean over the last 100 years. *J. Clim.* **2004**, *17*, 4485–4497. [CrossRef]
77. Screen, J.A.; Simmonds, I. The central role of diminishing sea ice in recent Arctic temperature amplification. *Nature* **2010**, *464*, 1334–1337. [CrossRef] [PubMed]
78. Comiso, J.C.; Hall, D.K. Climate trends in the Arctic as observed from space. *Wiley Interdiscip. Rev. Clim. Chang.* **2014**, *5*, 389–409. [CrossRef] [PubMed]
79. Dickson, R.R.; Osborn, T.J.; Hurrell, J.W.; Meincke, J.; Blindheim, J.; Adlandsvik, B.; Vinje, T.; Alekseev, G.; Maslowski, W. The Arctic Ocean response to the North Atlantic oscillation. *J. Clim.* **2000**, *13*, 2671–2696. [CrossRef]
80. Valchev, B. On the potential of small benthic foraminifera as paleoecological indicators: Recent advances. *Ann. UMG* **2003**, *46*, 51–56.
81. Chylek, P.; Folland, C.K.; Lesins, G.; Dubey, M.K.; Wang, M. Arctic air temperature change amplification and the Atlantic Multidecadal Oscillation. *Geophys. Res. Lett.* **2009**, *36*, L14801. [CrossRef]
82. Quadfasel, D.; SY, A.; Wells, D.; Tunik, A. Warming in the Arctic. *Nature.* **1991**, *350*, 385. [CrossRef]
83. Steele, M.; Boyd, T. Retreat of the cold halocline layer in the Arctic Ocean. *J. Geophys. Res. Ocean.* **1998**, *103*, 10419–10435. [CrossRef]
84. Greco, M.; Werner, K.; Zamelczyk, K.; Rasmussen, T.L.; Kucera, M. Decadal trend of plankton community change and habitat shoaling in the Arctic gateway recorded by planktonic foraminifera. *Glob. Chang. Biol.* **2021**, *28*, 1798–1808. [CrossRef]
85. Kaufman, D.S.; Schneider, D.P.; McKay, N.P.; Ammann, C.M.; Bradley, R.S.; Briffa, K.R.; Miller, G.H.; Otto-Bliesner, B.L.; Overpeck, J.T.; Vinther, B.M.; et al. Recent warming reverses long-term Arctic cooling. *Science* **2009**, *325*, 1236–1239. [CrossRef]